12-14-2013

A Non-Equilibrium, Pressure-Pressure Formulation for Air-Water Two-Phase Flow and Heat Transport in Porous Media

Amanda Meadows Hines

A non-equilibrium, pressure-pressure formulation for air-water two-phase flow and heat transport in porous media

By

Amanda Meadows Hines

A Thesis
Submitted to the Faculty of
Mississippi State University
in Partial Fulfillment of the Requirements
for the Degree of Master of Science
in Computational Engineering
in the Bagley College of Engineering

Mississippi State, Mississippi

December 2013

A non-equilibrium, pressure-pressure formulation

for air-water two-phase flow and heat transport

in porous media

By

Amanda Meadows Hines

Approved:

Edward A. Luke
(Major Professor)

Matthew W. Farthing
(Thesis Director)

J. Mark Janus
(Committee Member)

Roger King
(Graduate Coordinater)

Achille Messac
Dean
The James Worth Bagley
College of Engineering

Name: Amanda Meadows Hines

Date of Degree: December , 2013

Institution: Mississippi State University

Major Field: Computational Engineering

Major Professor: Dr. Edward A. Luke

Director of Thesis: Dr. Matthew W. Farthing

Title of Study: A non-equilibrium, pressure-pressure formulation for air-water two-phase flow and heat transport in porous media

Pages of Study: 49

Candidate for Degree of Master of Science

The detection of trace explosives in the subsurface is an active area of research for landmine detection. Understanding the air-water flow and heat transport phenomena in the subsurface plays an important role in improving chemical vapor detection. Implementing a finite element method that accurately captures water vapor transport in the vadose zone is still an open question. A non-equilibrium, pressure-pressure formulation has been implemented based on Smits, et al [22]. This implementation consists of four equations: a wetting phase (water) mass balance equation, a non-wetting phase (air) mass balance equation, a water vapor transport equation, and a heat transport equation.

This work will compare two implementations, a fully coupled approach and an operator splitting approach for the water vapor and heat transport equations. The formulation of the methods will be presented and the methods will be tested using collected data from physical experiments.

ACKNOWLEDGEMENTS

I would like to thank my major professor Dr. Edward A. Luke and my committee members Dr. Matthew W. Farthing and Dr. J. Mark Janus for their contributions and encouragement. I would especially like to thank Dr. Farthing for directing this work. I have learned so much from our many discussions throughout this process.

I would also like to thank Dr. Stacy E. Howington, Dr. Christopher E. Kees, and Dr. Steve C. Wilhelms for their time and advice. I wish to thank Dr. Kathleen M. Smits for her research in formulating the non-equilibrium model that forms the basis of this work as well as performing the physical and numerical experiments with which this work was compared.

The financial support for this work was provided by the US Army Corps of Engineers Engineer Research and Development Center under the 6.1 Military Engineering Basic Research Program.

I cannot find words to express my gratitude to my family for everything they have done for me. To my parents and sister, your love and support has made me the person I am today. Most importantly, thank you to my wonderful husband Joseph who is my foundation.

TABLE OF CONTENTS

LIST OF TABLES

LIST OF FIGURES

CHAPTER 1

INTRODUCTION

Soil moisture content and temperature play an important role in landmine detection. Therefore, the relationship between water vapor transport and temperature is an active area of research. Generally, the mass transfer between liquid water and water vapor is assumed to be instantaneous when modeling evaporation. However, Smits et al. [22] showed that the effects of non-equilibrium phase change are important in calculating mass and energy values. The non-equilibrium approach couples four equations, a mass balance equation for the wetting phase, a mass balance equation for the non-wetting phase, a water vapor transport equation, and a heat transport equation. This means that four unknowns must be solved for at each point in the domain. For 1D problems, the this approach appears reasonable. However, as we extend to 2D and 3D domains, the storage size and time taken to solve for the unknowns increase significantly.

The purpose of the work presented is to compare the fully coupled approach described by Smits et al. and a split operator approach where the water vapor transport and the heat transport equations are lagged behind the two-phase pressure-pressure equations. This reduces the number of unknowns to two for the pressure-pressure solve and one for the water vapor and heat transport solves. We will compare the time and accuracy of the two

approaches to determine if the split approach is a viable alternative to the fully coupled approach for this type of problem.

The remaining chapters in this thesis are outlined as follows. Chapter 2 provides background information used in formulating the equations for the non-equilibrium model. The formulations of the coupled partial differential equations of the continuous model are discussed in detail in Chapter 3. Chapter 4 provides the discrete approximations used to numerically solve the equations described in Chapter 3. The numerical experiments used to evaluate our research question are described in Chapter 5 and the results of the experiments are discussed in Chapter 6. Finally, Chapter 7 provides the conclusions drawn from this research as well as discussing some future directions for further research.

CHAPTER 2

BACKGROUND

The work presented for the non-equilibrium model consists of 4 equations shown below; a wetting phase continuity equation, a non-wetting phase continuity equation, a water vapor transport equation, and a heat transport equation.

$$\frac{\partial}{\partial t}\left(\theta_w \rho_w\right) + \nabla \cdot \left(-\rho_w \mathbf{Q}_w\right) = -\frac{R_{gw}}{\varrho_w^0} \tag{2.1}$$

$$\frac{\partial}{\partial t}\left(\theta_n \rho_n\right) + \nabla \cdot \left(-\rho_n \mathbf{Q}_n\right) = 0 \tag{2.2}$$

$$\frac{\partial}{\partial t}\left(\rho_n \theta_n \omega_v\right) + \nabla \cdot \left(\rho_n \omega_v \mathbf{Q}_n - D_v \rho_n \nabla \omega_v\right) = \frac{R_{gw}}{\varrho_w^0} \tag{2.3}$$

$$\frac{\partial}{\partial t}\left(\rho_b C_b T\right) + \nabla \cdot \left(C_n \rho_n T \mathbf{Q}_n + C_w \rho_w T \mathbf{Q}_w - \lambda_T \nabla T\right) = -\frac{L R_{gw}}{\varrho_w^0} - \frac{Q_s}{\varrho_w^0} \tag{2.4}$$

This chapter provides background information needed to formulate the equations used in this study.

2.1 Porous Media and Fluid Properties

2.1.1 Representative Elementary Volume

Fluid flow through porous media is impacted by the interconnection of its pores. In order to define macroscopic properties, such as porosity, hydraulic conductivity, etc., we need to choose a region that contains a representative sampling of the porous medium. This region is called a representative elementary volume (REV). The REV must be large

enough that properties are continuous but small enough not to introduce variability due to heterogeneity. Microscopic parameters are averaged over the REV to define macroscopic parameters that are independent of the REV itself [11].

2.1.2 Porosity

For this work, the REV consists of soil grains, a wetting phase, and a non-wetting phase where the non-wetting phase is made up of two components, dry air and water vapor. The ratio of the void volume to the overall volume of the REV is defined as the porosity of the medium and is therefore a dimensionless number. It is denoted as θ_s in this paper. Though porosity can vary over time due to compression, fracturing, etc., this work will focus on porosity as a function of space only, $\theta_s(\mathbf{x})$. We assume each porous medium has a constant porosity and therefore a change in porosity indicates a change in medium.

2.1.3 Molar Mass

Molar mass, sometimes referred to as molecular weight, is the amount of mass contained in one mole of a substance. It has units of mass per mole. The molar masses of water (M_w) and dry air (M_a) used in this work are $0.018\left[\frac{kg}{mol}\right]$ and $0.028\left[\frac{kg}{mol}\right]$ respectively.

2.1.4 Water Vapor Mass Fraction

The non-wetting phase used in this study is composed of dry air and water vapor as discussed previously. Therefore, the mass of the non-wetting phase is the sum of the water vapor mass and the dry air mass. The water vapor mass fraction (ω_n^v) is simply the mass of

the water vapor component divided by the mass of the non-wetting phase. Likewise, the dry air mass fraction (ω_n^a) is the mass of the dry air component divided by the mass of the non-wetting phase and the two fractions must sum to 1.

$$\omega_n^c = \frac{m_n^c}{m_n} \tag{2.5}$$

$$\sum_c \omega_n^c = 1 \tag{2.6}$$

$$c = v, a \tag{2.7}$$

The mole fractions of the water vapor (x_n^v) and dry air (x_n^a) components represent the amount of water vapor and dry air divided by the amount of the non-wetting phase. Like the mass fraction, the sum of the mole fractions must equal 1. The conversion between the mass fraction of component c and the mole fraction is defined as:

$$\omega_n^c = x_n^c \frac{M_n^c}{\sum_c x_n^c M_n^c} \tag{2.8}$$

2.1.5 Density

The density of a substance is the ratio of its mass divided by its volume and has units of mass per length cubed. For this work, we need to define densities for the wetting phase, the non-wetting phase, and the soil. The soil used in the numerical experiments listed below are homogeneous sands and therefore we assume the compressibility of the soil is negligible. This provides a constant density for the soil.

The density of the wetting phase is defined by Helmig [11] as:

$$\varrho_w = \frac{1}{\beta_p}\frac{\partial \varrho}{\partial p} + \frac{1}{\beta_T}\frac{\partial \varrho}{\partial T} \tag{2.9}$$

where β_p is the isothermal compressibility coefficient and β_T is the isobaric expansion coefficient. Due to its low compressibility, the pressure dependency can be neglected for the wetting phase [11]. Therefore, we will use Hillel's [12] definition of $\varrho_w(T)$:

$$\varrho_w = [1 - 7.37 \times 10^{-6}(T-4)^2 + 3.79 \times 10^{-8}(T-4)^3] \times 10^3 \tag{2.10}$$

where T is the temperature. This definition agrees well with the values listed in the Handbook of Chemistry and Physics [14] given our temperature range ($20 - 60^\circ$ C) as shown in Figure 2.1.

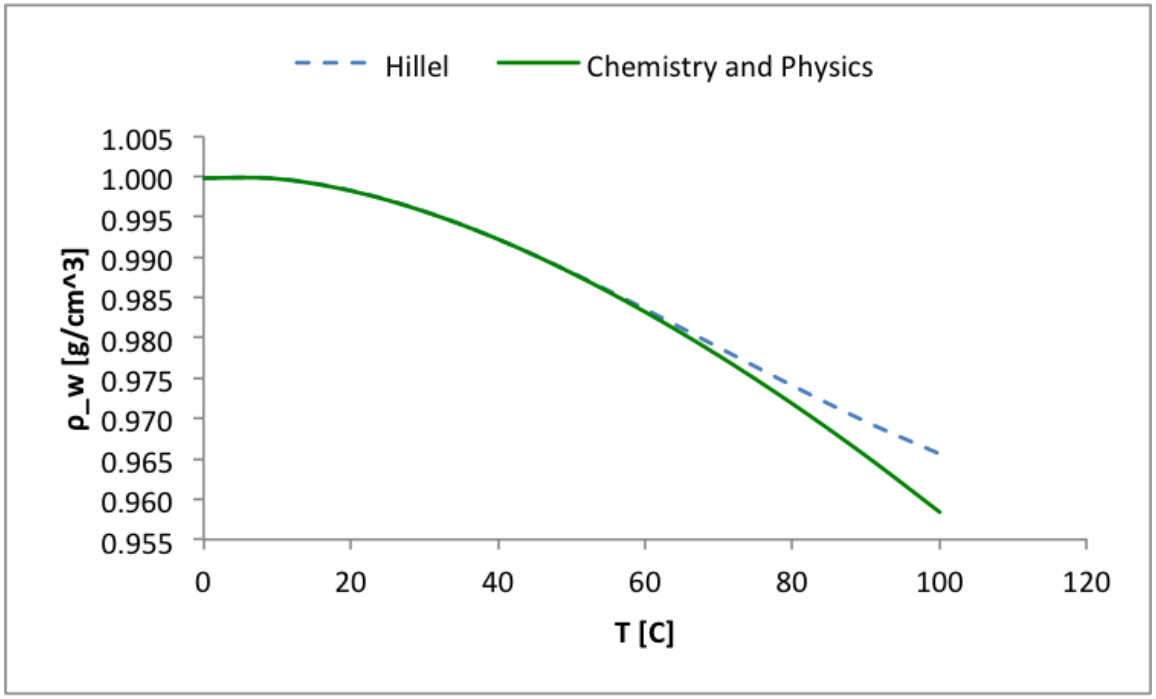

Figure 2.1

Wetting phase density $\left[\frac{g}{cm^3}\right]$ as it varies with temperature $[C]$

Unlike the wetting phase density, the non-wetting phase density varies with pressure, temperature, and water vapor as can be seen in Figure 2.2 and Figure 2.3. The non-wetting phase density mis the sum of the water vapor and dry air component densities. The non-wetting phase density can be defined using the molar form of the ideal gas equation.

$$\begin{aligned} \varrho_n &= \frac{p_n M_n}{RT} && (2.11) \\ M_n &= \left(\sum \frac{\omega_n^i}{M_n^i} \right)^{-1} && (2.12) \\ &= \left(\frac{\omega_v M_n^a + (1-\omega_v) M_n^v}{M_n^v M_n^a} \right)^{-1} \\ &= \left(\omega_v \frac{M_n^a - M_n^v}{M_n^a M_n^v} + \frac{1}{M_n^a} \right)^{-1} \end{aligned}$$

where R is the universal gas constant, p_n is the non-wetting phase pressure, $M_n^v = M_w$ is the molar mass of water vapor, $M_n^a = M_a$ is the molar mass of dry air, and ω_v is the mass fraction of water vapor in the non-wetting phase.

The density of water vapor in the non-wetting phase at saturation is know as the saturated vapor density. It is a function of temperature as discussed by Campbell [3]:

$$c_{vs} = exp\left(31.37 - \frac{6014.79}{T} - 7.92 \times 10^{-3} T\right) \frac{1}{T} \times 10^{-3} \qquad (2.13)$$

The dependence of the saturated vapor density on temperature can be seen in Figure 2.4.

2.1.6 Viscosity

The dynamic viscosity of a fluid is a measure of its resistance to shear stress and has units of mass per length per time. The more viscous a fluid is, the slower it flows with respect to a given shear stress. Due to the small variability of the viscosity of the non-wetting phase in the temperature range of our work ($20 - 60^\circ$ C), we assume a constant

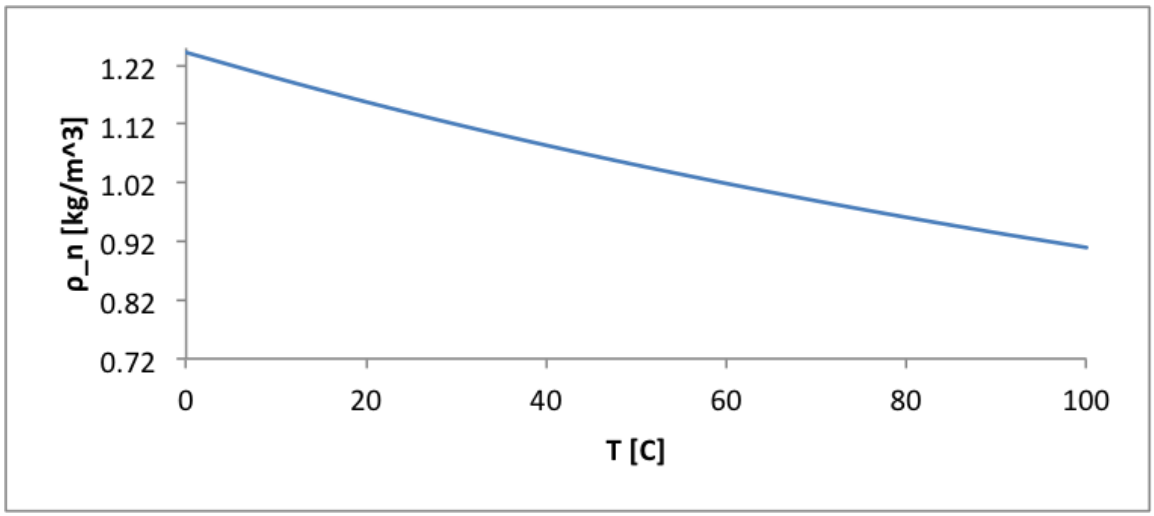

Figure 2.2

Non-wetting phase density as it varies with temperature at a given pressure with a set mass fraction of water vapor.

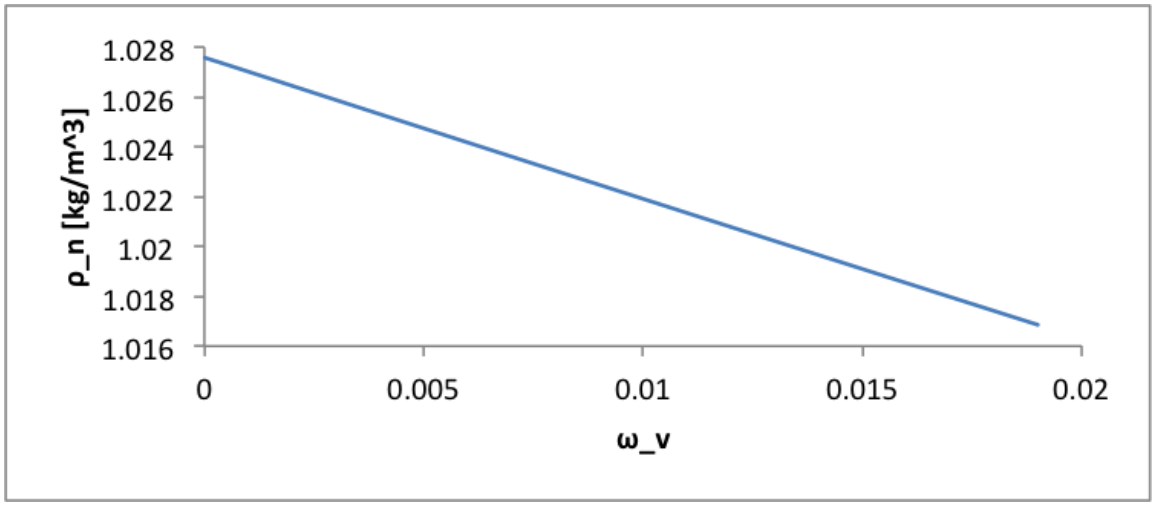

Figure 2.3

Non-wetting phase density as it varies with the water vapor mass fraction at a given pressure and temperature.

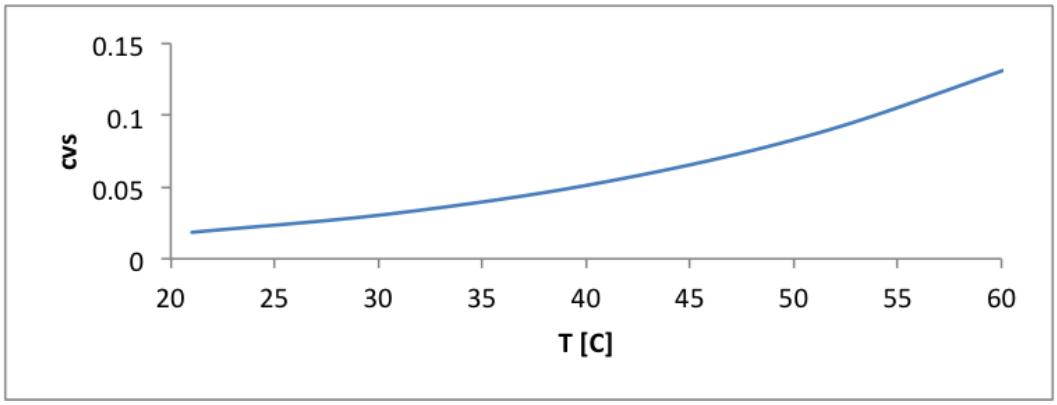

Figure 2.4

Saturated vapor density as a function of temperature.

non-wetting phase viscosity, μ_n. The wetting phase, however, does vary with temperature as Grifoll et al. [10] notes and can be seen in Figure 2.5.

$$\mu_w(T) = exp\left(-6.434 - \frac{2414}{T} + \frac{667,300}{T^2}\right) \tag{2.14}$$

2.1.7 Hydraulic Conductivity

The velocity at which a fluid moves through the soil is defined as the hydraulic conductivity and has units of length per time, $\bar{\boldsymbol{K}}$. The hydraulic conductivity tensor is symmetric and positive definite and is a combination of fluid and soil parameters. Splitting $\bar{\boldsymbol{K}}$ into its fluid and soil components for a single fluid phase, yields:

$$\bar{\boldsymbol{K}} = \frac{\bar{\boldsymbol{k}}\varrho g}{\mu} \tag{2.15}$$

where ϱ is the density of the fluid, μ is the viscosity of the fluid, g is gravity, and $\bar{\boldsymbol{k}}$ is the intrinsic permeability tensor of the medium which is related to grain size, grain diameter, grain packing, etc. [7].

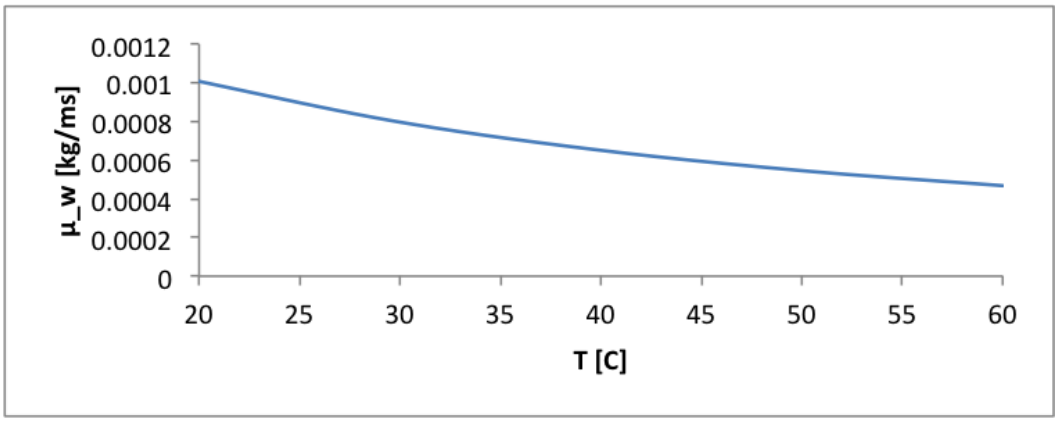

Figure 2.5

Wetting phase viscosity as it varies with temperature

2.1.8 Saturation

The saturation of a phase contained within a REV is a dimensionless variable and is defined as:

$$S_\alpha = \frac{\theta_\alpha}{\theta_s} \tag{2.16}$$

$$\sum_\alpha S_\alpha = 1 \tag{2.17}$$

where α is the fluid phase, θ_α is the volume fraction of the phase, and θ_s is the saturated volumetric wetting content. We make the assumption that the pore space can be completely filled by the wetting phase, thus the saturated volumetric wetting content is the porosity of the medium.

The residual volumetric wetting content, θ_{rw}, is the minimum wetting phase volume that remains after drainage of a soil due to soil properties such as pore connection, hetero-

geneity, etc. She et al. [21] defines the residual volumetric wetting content as a function of temperature:

$$\theta_{rw}(T) = \theta_{rw}(293K)\left[1 - c\left(T - 293K\right)\right] \tag{2.18}$$

where c is a fitting parameter with a weak dependence on soil type [10]. The dependence of θ_{rw} on temperature can be seen in Figure 2.6.

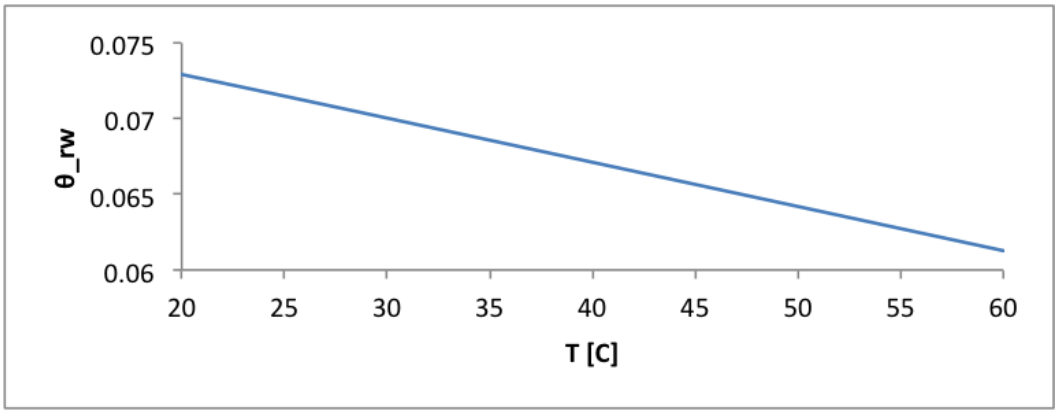

Figure 2.6

Residual wetting phase volume fraction as it varies with temperature.

2.1.9 Capillary Pressure

Capillary pressure (p_c) describes the pressure difference between two immiscible fluids (fluids that do not mix) due to inter-facial tension. It has units of force per area. For two-phase flow in porous media, the capillary pressure is the difference between the wetting

and non-wetting phase pressures and is related to the surface tension σ between the fluids and the pore structure [11]:

$$p_c = p_n - p_w \tag{2.19}$$

The dependence on pore structure indicates that capillary pressure is a function of saturation $p_c(S_w)$. This will be discussed in more detail in the following chapter.

Surface tension between the wetting and non-wetting phases is a function of temperature as noted by Saito et al. [20]:

$$\sigma = \left[75.6 - 0.1425\,(T - 273.15) - 2.38 \times 10^{-4}\,(T - 273.15)^2\right] \times 10^{-3} \tag{2.20}$$

Therefore, capillary pressure is a function of temperature. Grifoll et al. defines the temperature dependency of the capillary pressure as [10]:

$$p_c(S_w, T) = p_c(S_w, T_0)\frac{\sigma(T)}{\sigma(T_0)} \tag{2.21}$$

where T_0 is a reference temperature. These relationships are shown in Figure 2.7 and Figure 2.8.

2.1.10 Relative Humidity at Equilibrium

At equilibrium, the relative humidity is defined by the ratio of actual vapor pressure to saturated vapor pressure at a given temperature. Helmig defines the partial water vapor pressure using the Kelvin equation as [11]:

$$p_v = p_{sat}(T) exp\left(-\frac{(p_c - x^a p_n)\,M_w}{\varrho_w RT}\right) \tag{2.22}$$

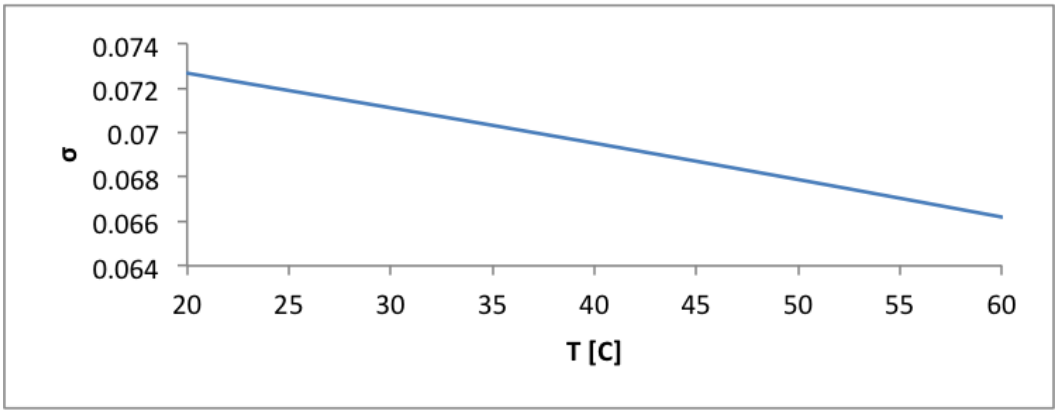

Figure 2.7

Surface tension (at a given wetting phase saturation) as it varies with temperature.

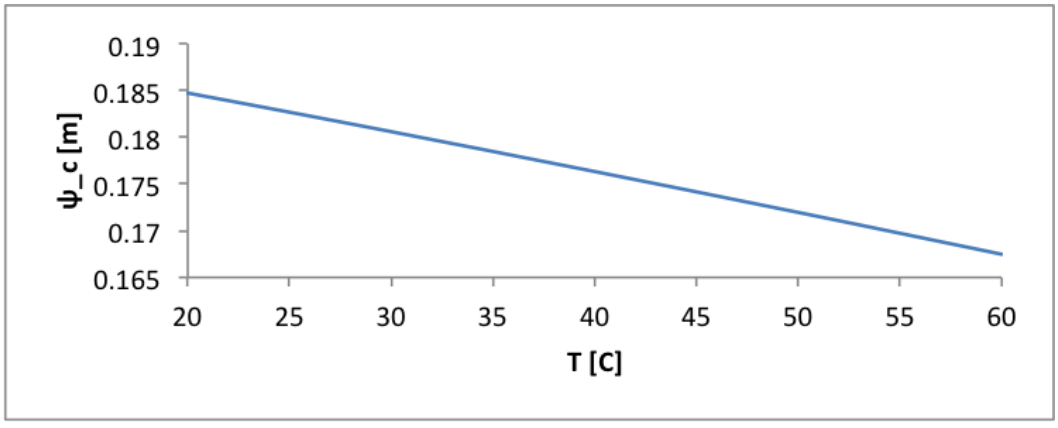

Figure 2.8

Capillary pressure (at a given wetting phase saturation) as it varies with temperature.

This gives:

$$H_{re} = \frac{p_v}{p_{sat}(T)} = exp\left(-\frac{(p_c - x^a p_n)\, M_w}{\varrho_w RT}\right) \tag{2.23}$$

The relationship between relative humidity at equilibrium, capillary pressure, and temperature can be seen in Figure 2.9 and Figure 2.10.

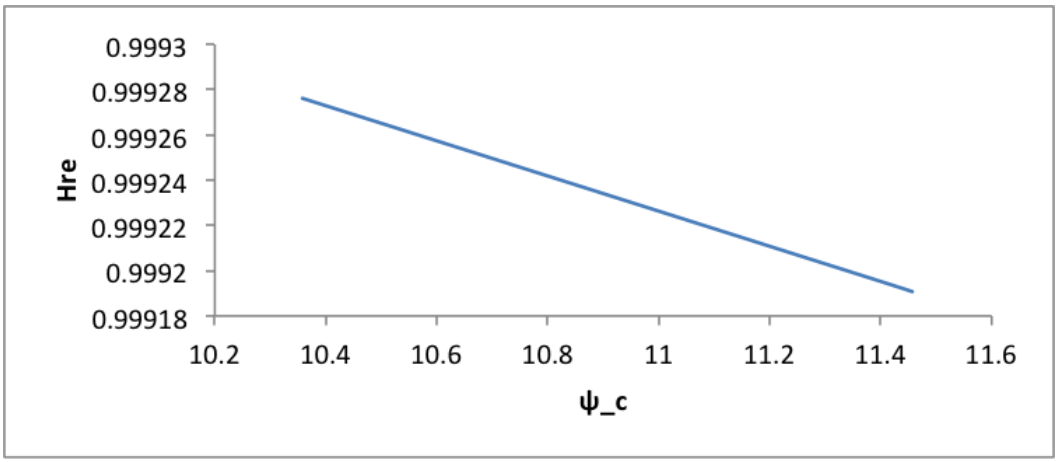

Figure 2.9

Change in relative humidity at equilibrium with respect to capillary pressure at a given temperature.

2.1.11 Vapor Enhancement Factor

In addition to advective mass flow in the subsurface, substances may also be transported through molecular diffusion. For this work, we are neglecting dispersion (convective mixing) in the gas phase. This type of transport was initially described using Fick's law:

$$F_c = -D_c \nabla(\varrho \omega_n^c) \tag{2.24}$$

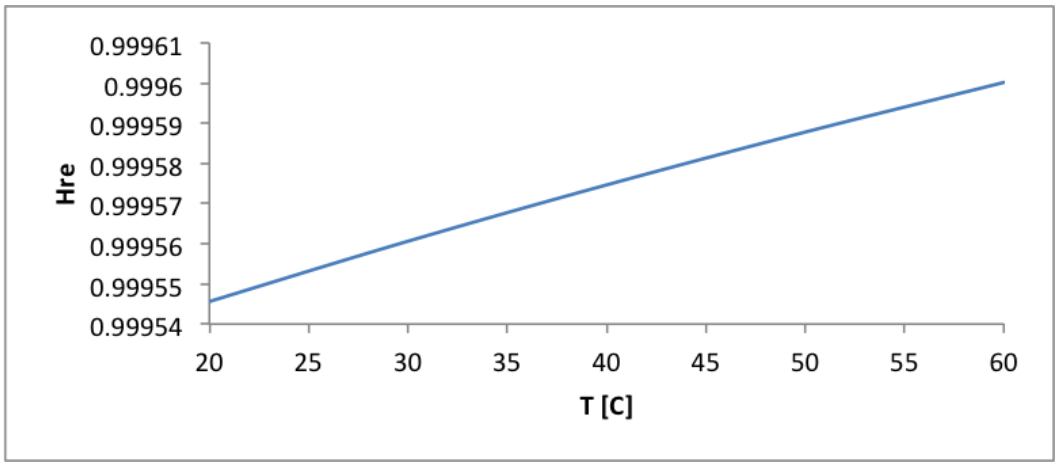

Figure 2.10

Change in relative humidity at equilibrium with respect to temperature at a given capillary pressure.

where F_c is the mass flux density of component c with units of mass times length squared per time, D_c is the diffusion coefficient for component c, and $\nabla(\varrho\omega_n^c)$ is the mass density gradient of component c. For this work, we are interested in water vapor diffusion in the subsurface. It has been shown that water vapor flow is affected by temperature gradients in soil and that modifications to Fick's law must be included to account for this dependence on temperature [4]. Much research has been conducted to determine what type of "enhancement factor" should be included to account for this type of flow.

This work focuses on the vapor enhancement factor defined by Cass et al. [4]:

$$\eta = A + B\frac{\theta_w}{\theta_s} - (A-1)exp\left(-\left[\left(1+\frac{2.6}{\sqrt{f_c}}\right)\frac{\theta_w}{\theta_s}\right]^3\right) \tag{2.25}$$

where A and B are fitting parameters and f_c is the fraction of clay. The clay fraction for our numerical experiments was zero since they used coarse sand. This simplifies the vapor enhancement factor, leaving us with:

$$\eta = A + B\frac{\theta_w}{\theta_s} \tag{2.26}$$

The effects of air pathways and tortuosity of the soil must also be accounted for in the diffusion coefficient. This work uses Penman's model to describe these effects $\tau = 0.66\theta_g$ [22]. Incorporating these factors gives the following water vapor diffusion coefficient:

$$D_v = D_a \tau \eta \tag{2.27}$$

where $D_a = 2.12 \times 10^{-}5(T/273.15)^2$ is the vapor diffusion coefficient in air as described by Campbell [3].

2.1.12 Mass Transfer between Liquid and Water Vapor

For the two-phase air-water system we are studying, the mass exchange term (R_{gw}) describes the mass transfer between liquid and water vapor and is defined as [1]:

$$R_{gw} = \frac{b\left(\theta_w - \theta_{rw}\right) RT}{M_w}\left(c_{vs} H_{re} - \varrho_n \omega_v\right) \tag{2.28}$$

where b is an empirical fitting parameter, R is the universal gas constant, T is the temperature, M_w is the molar mass of water, c_{vs} is the saturated vapor density in the gas phase, H_{re} is the relative humidity at equilibrium, ϱ_n is the density of the non-wetting phase, and ω_v is the mass fraction of water vapor in the air. At equilibrium, this term goes to zero as $\rho_n \omega_v \rightarrow c_{vs} H_{re}$. This term acts as a source/sink for three of the four equations.

2.1.13 Specific Heat

The specific heat of a substance is the amount of heat required to raise one unit of mass of the substance by one degree in temperature. The units of specific heat are energy per mass per temperature. The specific heat of water and air used for this work are $4459.15 \left[\frac{J}{kgK}\right]$ and $1003.5 \left[\frac{J}{kgK}\right]$ respectively.

2.1.14 Effective Thermal Conductivity

Thermal conductivity depends on several soil properties (quartz content, dry density, porosity) and fluid properties (saturation and water phase) [17]. It has units of energy per length per time per temperature. This work focuses on the modified Johansen model as described by Peters-Lidard:

$$\lambda_T = K_e \left(\lambda_{sat} - \lambda_{dry}\right) + \lambda_{dry} \tag{2.29}$$

$$\lambda_{dry} = \frac{0.135\gamma_d + 64.7}{2700 - 0.947\gamma_d}$$

$$\gamma_d = \left(1 - \theta_s\right) 2700$$

$$\lambda_{sat} = \lambda_s^{1-\theta_s} \lambda_w^{\theta_s}$$

$$\lambda_s = \lambda_{qz}^{q} \lambda_o^{1-q}$$

$$\lambda_o = \begin{cases} 2.0 & q > 0.2, \\ 3.0 & q <= 0.2 \end{cases}$$

$$K_e = \begin{cases} \log S_w + 1.0 & S_w > 0.1 \\ 0.0 & S_w <= 0.1 \end{cases}$$

where K_e is the Kersten number, λ_{sat} is the saturated thermal conductivity, λ_{dry} is the dry thermal conductivity, γ_d is the dry density of the soil, λ_s is the thermal conductivity of the solids in the soil, q is the quartz content, λ_{qz} is the thermal conductivity of quartz, and λ_o is the thermal conductivity of the other minerals in the soil.

In addition to the modified Johansen model, the split formulation was also run using the thermal conductivity model presented by Campbell et al.[3] shown below:

$$\lambda = \frac{k_w\theta_w\lambda_w + k_n\theta_n\lambda_n + k_s\theta_s\lambda_s}{k_w\theta_w + k_n\theta_n + k_s\theta_s} \tag{2.30}$$

$$\begin{aligned}
k_\alpha &= \frac{1}{3}\left[\frac{2}{1+\left(\frac{\lambda_\alpha}{\lambda_f}-1\right)g_a} + \frac{1}{1+\left(\frac{\lambda_\alpha}{\lambda_f}-1\right)g_c}\right] \\
\lambda_f &= \lambda_n + f_w\left(\lambda_w - \lambda_n\right) \\
f_w &= \frac{1}{1+\left(\frac{\theta_w}{\theta_w^o}\right)^{-q}} \\
\theta_w^0 &= 0.009 \\
g_a &= 0.1258 \\
g_c &= 1 - 2g_a \\
\lambda_w &= 0.554 + 2.24\times10^{-3}(T-273.15) - 9.87\times10^{-6}(T-273.15)^2 \\
\lambda_n &= 0.024 + 7.73\times10^{-5}(T-273.15) - 2.6\times10^{-8}(T-273.15)^2 \\
\lambda_s &= 7.52 \\
q &= q_0\left(\frac{T}{303}\right)^2 \\
q_0 &= 11.16
\end{aligned}$$

where k_α are weights for each of the components, λ_f is the fluid thermal conductivity, f_w is a weighting function, and λ_α are the thermal conducitivities of the components.

2.1.15 Latent Heat of Vaporization of Water

The process of phase change from liquid water to water vapor produces a drop in the surrounding temperature. The amount of energy needed to produce this phase change at a given pressure is defined as the latent heat of vaporization of water. Monteith and Unsworth describe the latent heat of vaporization as a function of temperature [15]:

$$L = 2.501 \times 10^6 - 2369.2(T - 273.15) \tag{2.31}$$

2.2 Multi-phase Continuity Equation

Given an REV, the change in fluid mass contained in the REV is equivalent to the mass flow of that fluid through the boundaries of the REV plus any mass change due to a source or sink. This is described mathematically by the conservation of mass equation:

$$\frac{\partial}{\partial t}\left(\theta_\alpha \varrho_\alpha\right) + \nabla \cdot \left(\varrho_\alpha \mathbf{Q}_\alpha\right) + \varrho_\alpha q_\alpha = 0 \qquad \alpha = n, w \tag{2.32}$$

where θ_α is the volume fraction of the phase, ϱ_α is the density of the fluid, $\mathbf{Q}$ is the vector of Darcy velocities (Q_x,Q_y,Q_z), and $\varrho_\alpha q_\alpha$ is a source/sink term. The sign of q_α is determined by whether the term represents a source or a sink.

2.3 Darcy's Law

Darcy's law is used to define fluid flow through porous media for low Reynolds numbers and a volumetric wetting content of $\theta_{rw} \leq \theta_w \leq \theta_s$. Darcy's law in one dimension is given by:

$$Q \;\; = -K\tfrac{dh}{dl} \tag{2.33}$$

where v is the Darcy velocity, K is the hydraulic conductivity, and $\frac{dh}{dl}$ is the hydraulic gradient. Darcy's law can be extended to three-dimensional flow [7], yielding the following:

$$Q_x = -K_{xx}\frac{\partial h}{\partial x} - K_{xy}\frac{\partial h}{\partial y} - K_{xz}\frac{\partial h}{\partial z} \tag{2.34}$$

$$Q_y = -K_{yx}\frac{\partial h}{\partial x} - K_{yy}\frac{\partial h}{\partial y} - K_{yz}\frac{\partial h}{\partial z} \tag{2.35}$$

$$Q_z = -K_{zx}\frac{\partial h}{\partial x} - K_{zy}\frac{\partial h}{\partial y} - K_{zz}\frac{\partial h}{\partial z} \tag{2.36}$$

or

$$\mathbf{Q} = -\bar{\boldsymbol{K}} \cdot \nabla h \tag{2.37}$$

where $\mathbf{Q}$ is the velocity vector, $\bar{\boldsymbol{K}}$ is the hydraulic conductivity tensor, and ∇h is the hydraulic gradient vector.

Extending Darcy's law to multi-phase flow [11], gives:

$$\mathbf{Q}_\alpha = -\frac{k_{r\alpha}\bar{\boldsymbol{k}}}{\mu_\alpha} \cdot (\nabla p_\alpha - \varrho_\alpha \mathbf{g}) \tag{2.38}$$

where μ_α is the viscosity of the phase, $k_{r\alpha}$ is the relative permeability of the phase, $\bar{\boldsymbol{k}}$ is the intrinsic permeability of the medium, ∇p_α is the pressure gradient of the phase, and ϱ_α is the density of the phase.

2.4 p-S-k relations

In order to use the multi-phase extension of Darcy's law shown above, we need to define the relative permeability of a phase $k_{r\alpha}$. Relative permeability is a function of saturation $k_{r\alpha}(S_\alpha)$. For Darcy flow, the effective saturation S_e can be defined as [13]:

$$S_e = \frac{\theta_w - \theta_{rw}}{\theta_s - \theta_{rw}} \qquad \theta_{rw} \leq \theta_w \leq \theta_s \tag{2.39}$$

Effective saturation is also related to capillary pressure p_c.

These relationships between capillary pressure, saturation, and relative permeability are generally known as p-S-k relations. Two commonly used p-S models for air-water systems were developed by Brooks and Corey (BC) [2] and van Genuchten (VG) [9].

The BC model, in addition to the Burdine theorem for relative permeability [11], relates effective saturation to capillary pressure using the following equations [13]:

$$S_e = \left(\frac{p_b}{p_c}\right)^{\lambda} \quad \text{for} \quad p_c \geq p_d \tag{2.40}$$

$$k_{rw} = (S_e)^{\frac{2+3\lambda}{\lambda}} \tag{2.41}$$

$$k_{rn} = (1 - S_e)^2 \left(1 - S_e^{\frac{2+\lambda}{\lambda}}\right) \tag{2.42}$$

where λ is related to the pore size distribution of the soil, $k_{rw}$and k_{rn} are the relative permeabilities of the wetting and non-wetting phases respectively, and p_b is the entry pressure for the soil. Since this model incorporates entry pressure into the equations, there exists a case where the capillary pressure is discontinuous at a material interface. Consider the case presented by Helmig [11] where the non-wetting phase flows from a soil with higher conductivity (I) to a soil of lower conductivity (II) and $p_{cI} < p_{dII}$. In this case, soil II is completely saturated with the wetting phase and the entry pressure for soil II has not been reached. This creates a discontinuity in the capillary pressure at the soil interface. This work focuses uses a continuous galerkin (CG) formulation therefore creating a need for a different p-S-k model than the BC model.

The VG model, unlike the BC model, does not produce a capillary pressure discontinuity in the case listed above. The discontinuity is avoided by setting the capillary pressure to

be 0 when $S_w = 1$. Therefore, the VG model is appropriate to use in our implementation. Also, the VG model is more widely used in vadose zone simulations for air-water where the entry effect is not as dramatic. The VG p-S relationship, in addition to the relative permeability definitions of Mualem

[16], are shown below [13]:

$$S_e = [1 + (\tilde{\alpha} \cdot |p_c|)^{\tilde{n}}]^{-\tilde{m}} \qquad \text{for} \quad p_c > 0 \tag{2.43}$$

$$k_{rw} = \sqrt{S_e}\left[1 - (1 - S_e^{\frac{1}{\tilde{m}}})^{\tilde{m}}\right]^2 \tag{2.44}$$

$$k_{rn} = \sqrt{1 - S_e}(1 - S_e^{\frac{1}{\tilde{m}}})^{2\tilde{m}} \tag{2.45}$$

where $\tilde{\alpha}$ is inversely proportional to the entry pressure, $\tilde{m}$ and $\tilde{n}$ are related to pore size distribution, and generally $\tilde{m} = 1 - \frac{1}{\tilde{n}}$.

2.5 Multi-phase Species Transport

Both water vapor and heat will be modeled using a continuity equation for multi-phase species transport. The general multi-phase species transport continuity equation is given by:

$$\frac{\partial}{\partial t}\left(\theta_\alpha \varrho_\alpha \omega_\alpha^i\right) + \nabla \cdot \left(\varrho_\alpha \omega_\alpha^i \mathbf{Q}_\alpha + \mathbf{j}_\alpha^i\right) = I_\alpha^i + R_\alpha^i + \mathcal{S}_\alpha^i \tag{2.46}$$

$$\begin{aligned}
\sum_{\alpha} \theta_{\alpha} &= 1 \\
\sum_{i} \omega_{\alpha}^{i} &= 1 \\
\sum_{i} \mathbf{j}_{\alpha}^{i} &= 0 \\
\sum_{i} \mathcal{S}_{\alpha}^{i} &= \mathcal{S}_{\alpha} \\
\sum_{\alpha} I_{\alpha}^{i} &= 0
\end{aligned}$$

where

$\alpha = w, n$ is the phase (wetting and non-wetting)

θ_{α} is the volume fraction of the phase

ϱ_{α} is the density of the phase

ω_{α}^{i} is the mass fraction of the species i in phase α

$\mathbf{v}_{\alpha}$ is the advective phase velocity

$\mathbf{j}_{\alpha}^{i}$ is the non-advective transport of species i in phase α

I_{α}^{i} is the inter-phase mass exchange term

R_{α}^{i} is the reaction term

$\mathcal{S}_{\alpha}^{i}$ is the source/sink term

Details of the coefficients for each equation will be discussed in the following chapter.

CHAPTER 3

FORMULATIONS

The work presented for the non-equilibrium-based model consists of 4 equations; a wetting phase continuity equation, a non-wetting phase continuity equation, a water vapor transport equation, and a heat transport equation. This chapter discusses the formulations of the equations.

3.1 Proteus

The work discussed has been implemented in the Proteus Computational Methods and Simulation Toolkit developed by the US Army Corps of Engineers Engineer Research and Development Center (ERDC). Proteus is a Python package designed to solve a set of nonlinear partial differential equations [18] of the form:

$$\frac{\partial m_i}{\partial t} + \nabla \cdot \left(\mathbf{f}_i - \sum_j^{n_c} \bar{\boldsymbol{a}}_{ij} \nabla u_j \right) + r_i + h_i \left(\nabla u \right) = 0, \quad i = 1, ..., n_c \tag{3.1}$$

where u is the primary variable, m_i is the accumulation term, $\mathbf{f}_i$ is the advective term, $\bar{\boldsymbol{a}}_{ij}$ is the diffusion coefficient tensor, r_i represents a source/sink or reaction term, and h_i is the Hamilton-Jacobi term. This equation is evaluated on a domain $\Omega \in \mathbb{R}^{n_d}$ where n_d is the number of dimensions and over the time interval $[0, t_f]$.

In order to solve the system of nonlinear partial differential equations, we must define boundary conditions as well as initial conditions (for time-dependent problems). The following is a list of boundary conditions available within Proteus:

$$u_j = u_j^b, \text{ on } \Gamma_j^D \tag{3.2}$$

$$-\bar{\boldsymbol{a}}_{ij}\nabla u_j \cdot \mathbf{n} = d_{i,j}^b, \text{ on } \Gamma_{i,j}^N \tag{3.3}$$

$$\boldsymbol{\sigma}_i \cdot \mathbf{n} = \sigma_i^b, \text{ on } \Gamma_i^T \tag{3.4}$$

where Γ is the boundary of the domain, Γ_j^D are the Dirichlet boundaries, $\Gamma_{i,j}^N$ are the Neumann boundaries, Γ_i^D are the total flux boundaries, and $\mathbf{n}$ is the unit outer normal to $\Gamma = \partial\Omega$ and

$$\boldsymbol{\sigma}_i = \mathbf{f}_i - \sum_{j=1}^{n_c} \bar{\boldsymbol{a}}_{ij}\nabla u_j \tag{3.5}$$

is the total flux for component i. Initial conditions are specified as $u_i(\mathbf{x}, t^0) = u_i^0(\mathbf{x})$.

3.2 Variational Form

Focusing on Equation (3.1), we see that it requires $u \in C^2(\Omega)$. This means that u, as well as its first and second partial derivatives, must be continuous on Ω [11]. The variational form allows us to relax this constraint so that $u \in C^1$. We will ignore the Hamilton-Jacobi term for our work. The first step is to multiply the equation by a test function w and integrate over Ω.

$$\int_\Omega \frac{\partial m_i}{\partial t} w + \int_\Omega \nabla \cdot \left(\mathbf{f}_i - \sum_j^{n_c} \bar{\boldsymbol{a}}_{ij}\nabla u_j \right) w + \int_\Omega r_i w = 0 \tag{3.6}$$

where the test function and its partial derivatives of order 1 are square integrable over the domain, $w \in H^1(\Omega)$.

Rearranging the equation yields:

$$\int_{\Omega} \nabla \cdot \left(\mathbf{f}_i - \sum_{j}^{n_c} \bar{\boldsymbol{a}}_{ij} \nabla u_j \right) w = - \int_{\Omega} \frac{\partial m_i}{\partial t} w - \int_{\Omega} r_i w \tag{3.7}$$

Applying the Divergence Theorem and integration by parts to the left hand side:

$$\begin{aligned} \int_{\Omega} \nabla \cdot \left(\mathbf{f}_i - \sum_{j}^{n_c} \bar{\boldsymbol{a}}_{ij} \nabla u_j \right) w &= \int_{\Omega} \left(\sum_{j}^{n_c} \bar{\boldsymbol{a}}_{ij} \nabla u_j - \mathbf{f}_i \right) \cdot \nabla w \\ &- \int_{\Gamma} w \left(\mathbf{f}_i - \sum_{j}^{n_c} \bar{\boldsymbol{a}}_{ij} \nabla u_j \right) \cdot \mathbf{n} \end{aligned} \tag{3.8}$$

Substituting back into Equation (3.7) produces the variational form of the equation

$$\begin{aligned} \int_{\Omega} \left(\sum_{j}^{n_c} \bar{\boldsymbol{a}}_{ij} \nabla u_j - \mathbf{f}_i \right) \cdot \nabla w &= \int_{\Gamma} w \left(\mathbf{f}_i - \sum_{j}^{n_c} \bar{\boldsymbol{a}}_{ij} \nabla u_j \right) \cdot \mathbf{n} \\ &- \int_{\Omega} \frac{\partial m_i}{\partial t} w - \int_{\Omega} r_i w \end{aligned} \tag{3.9}$$

The first term on the right hand side of Equation (3.9) is called a natural boundary condition since it occurs naturally in the variational form. Dirichlet boundary conditions can be handled in two ways, a strong form or a weak form. The strong form enforces the value of the primary variable to be equal to the boundary condition. For the weak form, the difference between the existing primary variable value and the boundary condition is multiplied by a penalty term and added to the diffusive flux.

3.3 Richards' Equation

Richards equation (RE) is a commonly used approach to solve two-phase flow in porous media [6]. The underlying assumption of RE is that the non-wetting phase maintains constant pressure throughout the domain [13]. Therefore, RE is formed by combining the

continuity equation and Darcy's law, Equations (2.32) and (2.38), for the wetting phase. This gives:

$$\frac{\partial}{\partial t}\left(S_w\theta_s\varrho_w\right) + \nabla\cdot\left[-\varrho_w\frac{k_{rw}\bar{\boldsymbol{k}}}{\mu_w}\left(\nabla p_w - \varrho_w\mathbf{g}\right)\right] + \varrho_w q_w = 0 \tag{3.10}$$

Equation (3.10) is the non-dimensionalized mixed form of RE (MRE). It is called the mixed form because the equation contains both pressure head and saturation terms. RE can be written such that it only contains pressure head terms or saturation terms. The pressure head version of RE is shown below:

$$C(p_w)\tfrac{\partial p_w}{\partial t} + \nabla\cdot\left[-\varrho_w\tfrac{k_{rw}\bar{\boldsymbol{k}}}{\mu_w}\left(\nabla p_w - \varrho_w\mathbf{g}\right)\right] + \varrho q_w = 0 \tag{3.11}$$

$$C(p_w) = \varrho_w S_w\tfrac{\partial\theta_s}{\partial p_w} + \varrho_w\theta_s\tfrac{\partial S_w}{\partial p_w} + \theta_s S_w\tfrac{\partial\varrho_w}{\partial p_w} \tag{3.12}$$

where $C(\psi_w)$ is called the specific moisture capacity function [5]. Likewise, the saturation version is formed by:

$$\frac{\partial}{\partial t}(S_w\theta_s\varrho_w) + \nabla\cdot\left[-\varrho_w\frac{k_{rw}\bar{\boldsymbol{k}}}{\mu_w}\left(\frac{1}{C(p_w)}\nabla(S_w\theta_s\varrho_w) - \varrho_w\mathbf{g}\right)\right] + \varrho_w q_w = 0 \tag{3.13}$$

Each version of RE has its strengths and weaknesses. The saturation form conserves mass but can not be used when the soil is fully saturated. Also, there are situations where the saturation becomes discontinuous as stated above. The pressure head form does not conserve mass but is more suitable for heterogeneous media. However, instabilities arise when the pressure head form is used to simulate infiltration into an initially dry domain due to the nonlinearity of the specific capacity term [5]. The mixed form of RE combines the mass conservation of the volume fraction form with the flexibility of the pressure head form. However, mass lumping of the time term is needed to generate good approximations when using the finite element approach to approximate the mixed form [5].

3.4 Two-phase Formulations

As stated previously, RE only models the wetting phase flow through a domain since the non-wetting phase in the unsaturated zone is assumed to be infinitely mobile [19]. Equation (2.32) can be modified to model both the wetting and non-wetting phases:

$$\frac{\partial}{\partial t}\left(S_\alpha \theta_s \varrho_\alpha\right) + \nabla \cdot \left[-\varrho_\alpha \frac{k_{r\alpha}\bar{\boldsymbol{k}}}{\mu_\alpha}\left(\nabla p_\alpha - \varrho_\alpha \mathbf{g}\right)\right] + \varrho_\alpha q_\alpha = 0 \qquad \alpha = n, w \tag{3.14}$$

This yields two equations and four unknowns, $S_w, p_w, S_n,$ and p_n. The number of unknowns can be reduced to two through the use of Equations (2.16), (2.17), and (2.19), and the VGM parameters described in equations Equations (2.43), (2.44), and (2.45). The choice of independent variables provides different formulations for the two-phase model.

3.4.1 Pressure-Saturation (PS) Formulation

For the PS formulation, one pressure term and one saturation term are chosen as the independent variables. Choosing the wetting phase pressure p_w and the wetting phase saturation S_n as the primary variables, the following substitutions are necessary:

$$p_n = p_w + p_c \tag{3.15}$$

$$S_n = 1 - S_w \tag{3.16}$$

into the general equations yielding the following set of coupled equations:

$$\frac{\partial}{\partial t}\left[\theta_s S_w \rho_w\right] + \nabla \cdot \left[-\rho_w \bar{\boldsymbol{K}}_{ew}\left(\nabla \psi_w - \rho_w \mathbf{g}_u\right)\right] + \rho_w q_w = 0 \tag{3.17}$$

$$\frac{\partial}{\partial t}\left(\theta_s (1 - S_w)\rho_n\right) + \nabla \cdot \left[-\rho_n \frac{\bar{\boldsymbol{K}}_{en}}{\hat{\mu}_n}\left[\nabla\left(\psi_c + \psi_w\right) - \rho_n \mathbf{g}_u\right]\right] + \rho_n q_n = 0 \tag{3.18}$$

$$
\begin{aligned}
\varrho_w &= \varrho_w^0 e^{\gamma(\psi-\psi_w^0)} \\
\rho_w &= \frac{\varrho_w}{\varrho_w^0} \\
\psi_w &= \frac{p_w}{\varrho_0 \|\mathbf{g}\|} \\
\mathbf{g}_u &= \frac{\mathbf{g}}{\|\mathbf{g}\|} \\
\bar{\boldsymbol{K}}_e &= k_{r\alpha}\bar{\boldsymbol{K}}_s \\
\bar{\boldsymbol{K}}_s &= \frac{\varrho_0 \|\mathbf{g}\| \bar{\boldsymbol{k}}}{\hat{\mu}_w} \\
\hat{\mu}_n &= \frac{\mu_n}{\mu_w^0} \\
\hat{\mu}_n &= \frac{\mu_w}{\mu_w^0}
\end{aligned}
$$

where ψ_w is the pressure head, ψ_w^0 is a reference pressure head, ϱ_w^0 is a reference density with respect to ψ_w^0, γ describes the compressibility of the wetting phase, $\bar{\boldsymbol{K}}_e$ is the effective hydraulic conductivity, $\bar{\boldsymbol{K}}_s$ is the saturated conductivity, $\|\mathbf{g}\|$ is the norm of the gravitational acceleration vector $\mathbf{g}$, and μ_w^0 is a reference viscosity.

3.4.2 Pressure-Pressure (PP) Formulation

For the PP formulation, two pressure variables are chosen as the independent variables. This work will focus on the wetting phase pressure p_w and the capillary pressure p_c as the primary variables. Therefore the PP formulation yields the following coupled equations:

$$
\frac{\partial}{\partial t}\left(\theta_s S_w \rho_w\right) + \nabla \cdot \left[-\rho_w \bar{\boldsymbol{K}}_{ew}\left(\nabla\psi_w - \rho_w \mathbf{g}_u\right)\right] + \rho_w q_w = 0 \tag{3.19}
$$

$$
\frac{\partial}{\partial t}\left(\theta_s S_n \rho_n\right) + \nabla \cdot \left(-\rho_n \frac{\bar{\boldsymbol{K}}_{en}}{\hat{\mu}_n}\left[\nabla\left(\psi_w + \psi_c\right) - \rho_n \mathbf{g}_u\right]\right) + \rho_n q_n = 0 \tag{3.20}
$$

Equations (3.19) and (3.20) can both be written in the general form of Equation (3.1) where:

$$
\begin{aligned}
m_w &= \theta_s S_w \rho_w \\
m_n &= \theta_s S_n \rho_n \\
\mathbf{f}_w &= \rho_w^2 \bar{\boldsymbol{K}}_{ew} \mathbf{g}_u \\
\mathbf{f}_n &= \rho_n^2 \frac{\bar{\boldsymbol{K}}_{en}}{\hat{\mu}_n} \mathbf{g}_u \\
\bar{\boldsymbol{a}}_w &= \rho_w \bar{\boldsymbol{K}}_{ew} \\
\bar{\boldsymbol{a}}_n &= \rho_n \frac{\bar{\boldsymbol{K}}_{en}}{\hat{\mu}_n} \\
\phi_w &= \psi_w \\
\phi_n &= \psi_w + \psi_c \\
r_w &= \rho_w q_w \\
r_n &= \rho_n q_n
\end{aligned}
$$

3.5 Water Vapor Transport

The water vapor transport equation follows the multi-phase species transport equation listed in the previous chapter.

$$\frac{\partial}{\partial t}\left(\varrho_n \theta_n \omega_v\right) + \nabla \cdot \left(\varrho_n \omega_v \mathbf{Q}_n - D_v \varrho_n \nabla \omega_v\right) = R_{gw} \tag{3.21}$$

where ω_v is the water vapor mass fraction and D_v is the effective vapor diffusion coefficient as described in the previous chapter. Non-dimensionalizing gives:

$$\frac{\partial}{\partial t}\left(\rho_n \theta_n \omega_v\right) + \nabla \cdot \left(\rho_n \omega_v \mathbf{Q}_n - D_v \rho_n \nabla \omega_v\right) = \frac{R_{gw}}{\varrho_w^0} \tag{3.22}$$

3.6 Heat Transport Equation

The heat transport equation, like the water vapor transport equation, is a continuity equation for multi-phase species transport.

$$\frac{\partial}{\partial t}\left(\varrho_b C_b T\right) + \nabla \cdot \left(C_n \varrho_n T \mathbf{Q}_n + C_w \varrho_w T \mathbf{Q}_w - \lambda_T \nabla T\right) = -LR_{gw} - Q_s \tag{3.23}$$

$$\varrho_b = \varrho_w \theta_w + \varrho_n \theta_n + \varrho_s \theta_s \tag{3.24}$$

$$C_b = \frac{\varrho_w \theta_w C_w + \varrho_n \theta_n C_n + \varrho_s \theta_s C_s}{\varrho_w \theta_w + \varrho_n \theta_n + \varrho_s \theta_s} \tag{3.25}$$

$$L = 2.501 \times 10^6 - 2369.2(T - 273.15) \tag{3.26}$$

$$Q_s = h 2\pi r \triangle T \tag{3.27}$$

where ϱ_b is the density of the mixture (soil+water+air), C_b is the specific heat of the mixture (soil + water + air), C_α is the specific heat of the phase (solid,wetting,non-wetting), λ_T is the effective thermal conductivity, L is the latent heat coefficient, Q_s is the heat loss estimated from Newton's law of cooling, and h is the height of the column. Non-dimensionalizing gives:

$$\frac{\partial}{\partial t}\left(\rho_b C_b T\right) + \nabla \cdot \left(C_n \rho_n T \mathbf{Q}_n + C_w \rho_w T \mathbf{Q}_w - \lambda_T \nabla T\right) = -\frac{LR_{gw}}{\varrho_w^0} - \frac{Q_s}{\varrho_w^0} \tag{3.28}$$

$$\rho_b = \rho_w \theta_w + \rho_n \theta_n + \rho_s \theta_s \tag{3.29}$$

$$C_b = \frac{\rho_w \theta_w C_w + \rho_n \theta_n C_n + \rho_s \theta_s C_s}{\rho_w \theta_w + \rho_n \theta_n + \rho_s \theta_s} \tag{3.30}$$

$$\tag{3.31}$$

CHAPTER 4

DISCRETE APPROXIMATIONS

Solutions to the boundary value problems (BVP) listed in the previous chapter are approximated using the continuous Galerkin finite element method. The method consists of converting strong BVPs to their variational form and approximating the infinite dimensional problem as a finite dimensional problem by defining a set of basis functions and using a subspace of piecewise polynomial functions. This chapter discusses the implementation of method for the numerical experiments.

4.1 Spatial Discretization

The numerical experiments presented were spatially discretized using 1D elements, or lines. The domain Ω was partitioned into n elements, e_i where $i = 1, 2, ..., N_e$ and each element consisted of two nodes, $x_{e_{i,1}}$ and $x_{e_{i,2}}$. This gives the following spatial discretization:

$$E_h = \left\{ e_i | \cup_{i=1}^{N_e} = \Omega \text{ and } e_i \cap e_j = \emptyset \text{ if } i \neq j, 1 \leq i, j \leq N_e \right\} \tag{4.1}$$

4.1.1 Basis Functions

Here we review the basic discretiziation for the finite element method. For simplicity we will use the general form from Equation (3.1) to describe our set of equations. We wish to find a solution, $\hat{u}$, such that

$$\int_{\Omega} \left[\frac{\partial m_i}{\partial t} w + \nabla \cdot \left(\mathbf{f}_i - \sum_{j}^{n_c} \bar{\boldsymbol{a}}_{ij} \nabla \hat{u}_j \right) w + r_i w \right] dx = 0 \tag{4.2}$$

for $\hat{u} \in V$ and all $w \in W$ where $V, W \in H^1(\Omega)$, $\hat{u} = u^b$ on Γ^D, and $w = 0$ on Γ^D. In order to find an approximation $\hat{u}$ of u from the space $H^1(\Omega)$, a finite dimensional subspace for w and $\hat{u}$ must be chosen. For this work, the finite dimensional subspace P_h^1 was chosen for both subspaces consisting of piecewise linear functions on the given discretization E_h.

Given a function $u \in P_h^1$, $u(x) = a_i + b_i x$ for each edge $e_i \in E_h$, a Lagrange basis, also known as a nodal basis, was chosen such that:

$$N_i(x_j) = \begin{cases} 1 & i = j, \\ 0 & i \neq j \end{cases} \tag{4.3}$$

An approximation of u from P_h^1, defined as $\hat{u}$, can then be written as:

$$\hat{u} = \sum_{i=1}^{N_n} c_i N_i(x_j) \tag{4.4}$$

where c_i is a vector of the nodal values of function w. The trial function v also belongs to the same subspace, $v \in P_h^1 = W$.

4.1.2 Quadrature Points

A quadrature rule was used to approximate the integrals listed in the general equation for each edge e_i. For stability purposes, mass lumping was done by using the Gauss-

Lobatto quadrature rule. Given a function f on each edge of the mesh e_i, the integration of the function was approximated using the 2 point Gauss-Lobatto quadrature rule:

$$\int_{\Omega} f \, \mathrm{d}x \approx \sum_{e \in E_h} \sum_{i=1}^{N_q} \Delta x_e 0.5 * f(x_{e,i}) \tag{4.5}$$

where $N_q = 2$ is the number of quadrature points per edge, Δx_e is the change in x over the element e, 0.5 is the weight at each quadrature point, and $f(x_{e,i})$ is the value of the function at the quadrature point $x_{e,i}$.

4.1.3 Reference Element

Using a reference element for approximations is beneficial since it allows us to compute the basis functions and their gradients only once. The reference element used for this work is the line defined by endpoints $x_{e_i,0} = 0.0$ and $x_{e_i,1} = 1.0$. The mapping from the reference element to an arbitrary element in the mesh is defined as:

$$x = x_1 + (x_2 - x_1) x_{e_i} \tag{4.6}$$

4.2 Time Discretization

The change in the accumulation term over time for the numerical experiments was discretized using the Backward Euler scheme.

$$m_i^{n+1} = \frac{m_i^{n+1} - m_i^n}{\Delta t} \tag{4.7}$$

where Δt is the time step size and i is the order of the method, in this case $i = 1$. The scheme is classified as an implicit scheme because the solution at m^{n+1} depends on the evaluation of the function at the $n + 1$ time step. The Backward Euler scheme is a first order scheme.

4.3 Solvers

4.3.1 Nonlinear Solver

Equation (3.1) results in a discrete nonlinear system of equations where we are trying to solve $\mathbf{R}(\mathbf{u}) = 0$. The Newton-Raphson method, also referred to as Newton's method, was used to linearize the nonlinear system of equations. Newton's method provides the following set of linear equations:

$$\bar{\boldsymbol{A}}\Delta\mathbf{u} = -\mathbf{R} \tag{4.8}$$

where A contains the approximations of the jacobian, $\Delta\mathbf{u} = \mathbf{u}^{n+1,k+1} - \mathbf{u}^{n+1,k}$ is the increment in the solution, $\mathbf{R}(\mathbf{u}^{n+1,k})$ contains the residual, and k is the iteration step. Though Newton's method formally provides quadratic conversion, it requires that the guess is close enough to the solution. We include line searches to improve the robustness of Newton's method.

4.3.2 Linear Solver

The system of linear equations generated by Newton's method was then solved using a sparse direct LU decomposition. For this work, the LU decomposition is performed using the SuperLU library.

4.3.3 Split Operator

The sequential split operator (SSO) method with a fixed timestep size was used for this work. The fully coupled equations were decoupled into 3 solves, first the wetting phase and non-wetting phase mass balance solve, second the water vapor transport solve, and finally the heat transport solve. The SSO method works by solving the first subproblem over the

timestep, then solving the next subproblem over the timestep using the values from the first solve, and finally solving the third subproblem over the timestep using the values from the first two solves. The SSO method is a first order splitting method [8].

CHAPTER 5

NUMERICAL EXPERIMENTS

The two formulations were tested using the domain and boundary conditions described by Smits, et. al [22]. The global parameters used in the simulation are listed in Table 5.1 and the material properties for the sand are listed in Table 5.2. The 1.1 meter column consisted of 1101 nodes and 1100 elements(lines) producing a spacing of 1 millimeter. The domain started out almost completely saturated (99.996%) with the wetting phase. No flow boundary conditions were applied at the top and bottom of the column for the wetting phase. The non-wetting phase boundary consisted of no flow at the bottom and a dirichlet condition of atmospheric pressure at the top. For temperature, the bottom boundary condition was fixed at 22°C and a time-dependent temperature boundary condition was assigned at the top. For the water vapor transport, no flow was assigned at the bottom and a time-dependent water vapor mass fraction was calculated at the top from observed relative humidities.

For initial conditions, the wetting phase was set to hydrostatic pressure, the capillary pressure was set such that the saturation was 99.996% throughout the column, the temperature was set to 22°C, and the water vapor mass fraction was set to the saturated vapor mass fraction given the set temperature.

Table 5.1

Global Parameters

Parameter	Value	Units
ϱ_{w_0}	998.2	kg/m^3
ϱ_{n_0}	1.205	kg/m^3
μ_w	8.9e-4	kg/ms
μ_n	1.81e-5	kg/ms
g	9.8	m/s^2
Mw	1.8e-2	kg/mol
Mn	2.8e-2	kg/mol
R	8.314	$J/molK$

Table 5.2

Sand Properties

Property	Sand (30/40)	Units
s_{rw}	0.0838	-
s_s	1.0	-
ω	0.334	-
$\mathbf{k}$	1.063e-7	m^2
α	5.7	-
n	17.8	-
ϱ_s	2650	kg/m^3
C_s	730	J/kgK
q_c	0.998	-
λ_{dry}	0.3	W/mK
λ_{sat}	2.9	W/mK

CHAPTER 6

RESULTS

For the convergence tests, a series of three runs were made with both the fully coupled and split approaches using progressively smaller timestep sizes. The timestep sizes used were 1, 2, and 4 seconds. The results of these runs were compared with the baseline run of timestep size 0.01 seconds and the errors were normalized by the column height. The series simulated 30 minutes of time using initial conditions generated from the fully coupled base run at 15 minutes.

6.0.4 Convergence Tests

The Backward Euler method is a first order method. Therefore, as the the timestep size is cut in half, the error should also be cut in half. Figure 6.1 shows the error rate with respect to timestep size normalized by the column height for the fully coupled approach. The chart shows that the slope for each of the components is approximately 1.0. Likewise, the slope for each of the components for the split formulation when compared to the split formulation baseline is approximately one as can be seen in Figure 6.2.

The SSO method is also order one. Figure 6.3 shows the split solution minus the fully coupled solution at each timestep size. Though the errors are decreasing, the slopes are not 1 like the previous two figures. The slopes range from 0.4 to 0.8 for the components. This

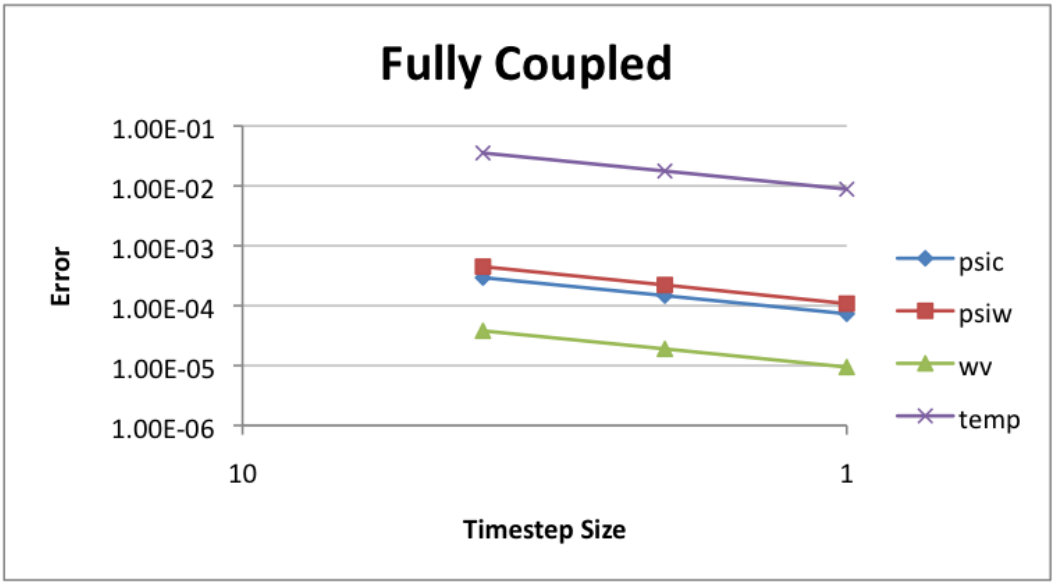

Figure 6.1

L2-norm calculated by subtracting the fully coupled solution from the base solution for each timestep size.

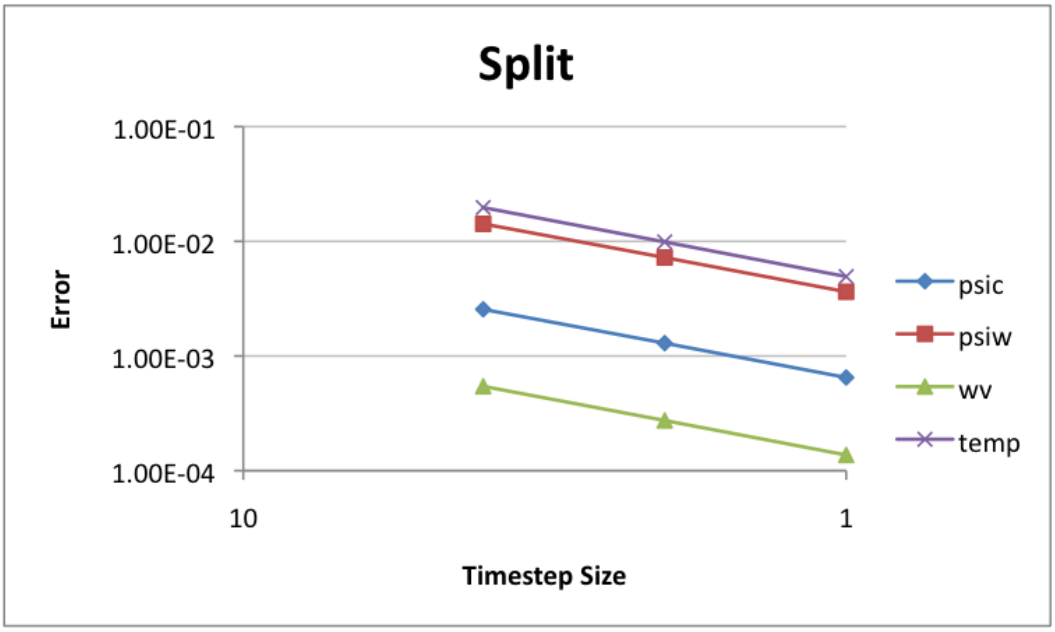

Figure 6.2

L2-norm calculated by subtracting the split solution from the base solution for each timestep size.

indicates that the splitting error is large enough to effect the temporal convergence rate. The errors between the two baselines ranged from 1.9e-4 to 7.6e-3.

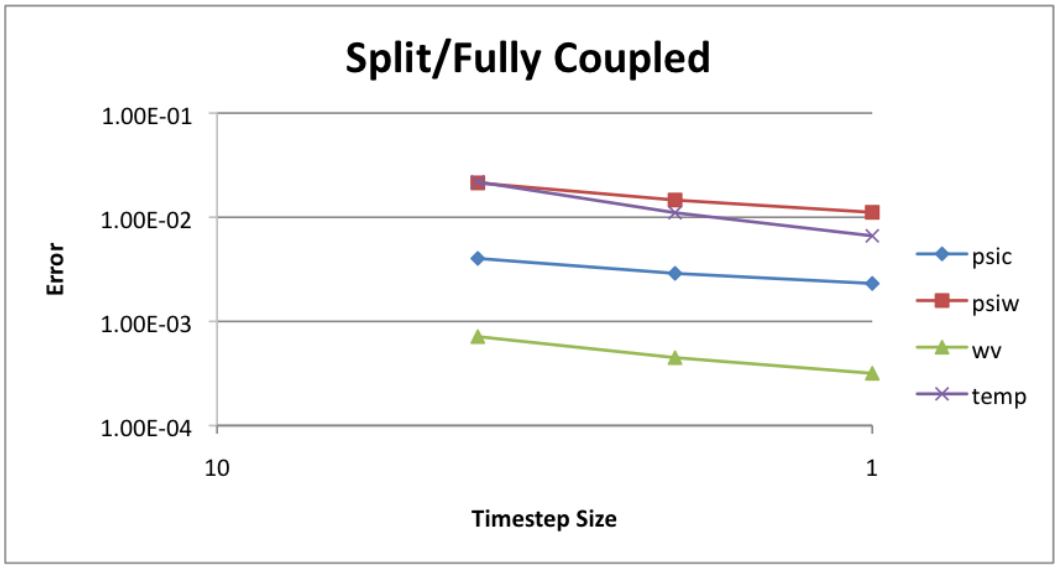

Figure 6.3

L2-norm calculated by subtracting the split solution from the fully coupled solution for each timestep size.

Figure 6.4 shows the wetting phase pressure error with respect to CPU time for the different timestep sizes. The wetting phase pressure was chosen because it has the highest error when comparing the split minus fully coupled approaches. The figure shows, as expected, that the split formulation is faster for a given timestep size but incurs a larger error. The fully coupled approach takes approximately 3.5 times longer to run than the split approach. As discussed previously, the splitting error negatively affects the convergence rate. For the wetting phase pressure, the slope is approximately 0.5.

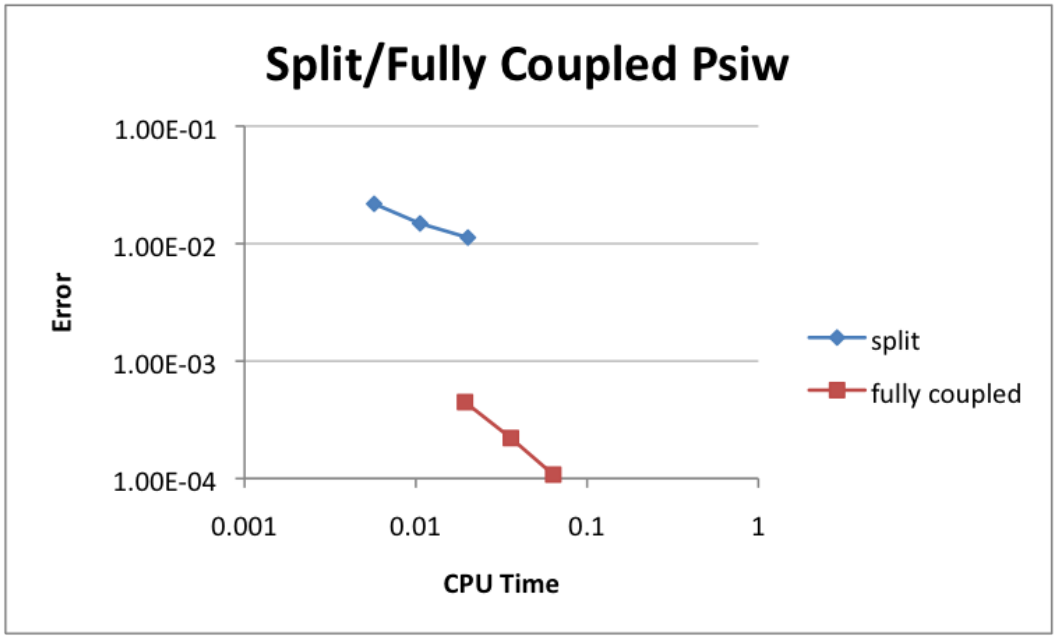

Figure 6.4

L2-norm and CPU time for each timestep size.

6.0.5 Comparisons with Observed and Smits Simulations

The fully coupled and split approaches are compared against Smits et al. simulation results and observed data. Two temperature plots are shown, 1 hour and 1 day. The saturations in the column were compared at 12 hours and 1 day. All four plots, show that the fully coupled approach and split approach are in good agreement.

The charts show that for each comparison, both approaches capture the shape of the curves. The temperature plots show a divergence between my simulation results and those of Smits et. al. Two split formulation results are shown, one using the Johansen thermal conductivity model and the other using the Campbell et al. thermal conductivity model which Smits et al. used. Even with the divergence in temperatures, there is good agree-

ment between the simulated saturation results. It appears that for our implementation, the Johansen model better matches the observed and simulated data of Smits et al.

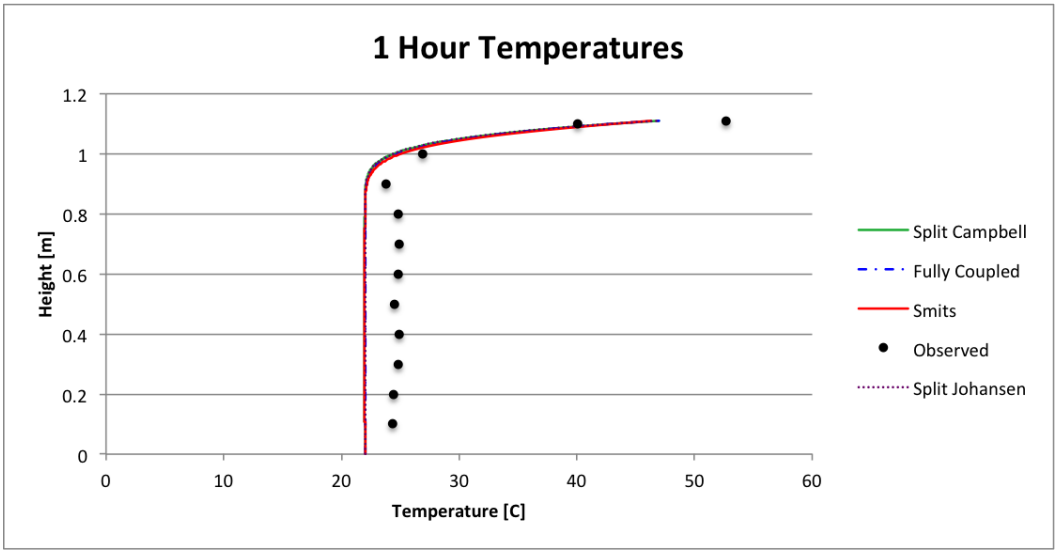

Figure 6.5

Fully coupled and split simulated data compared to Smits simulated and observed data at 1 hour.

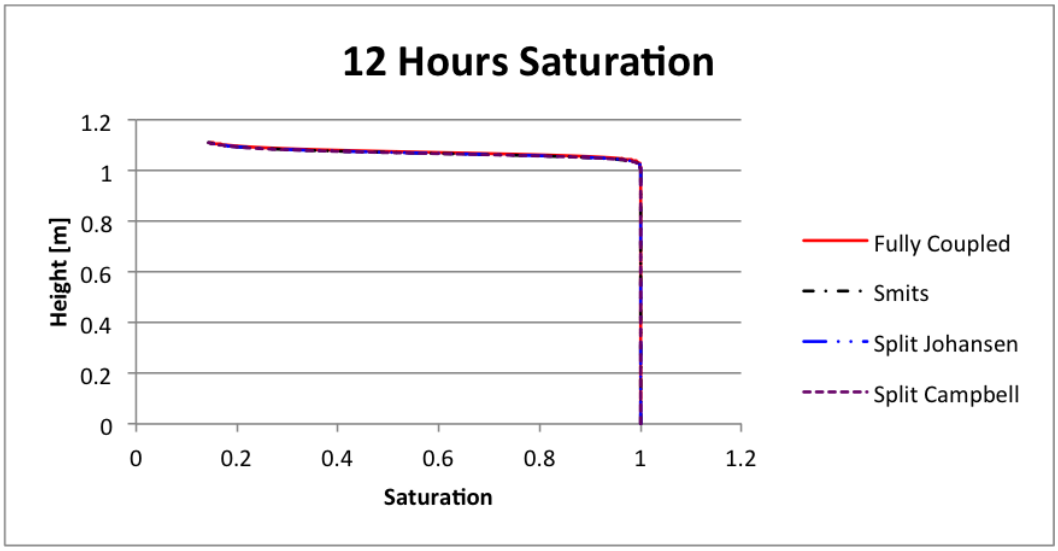

Figure 6.6

Fully coupled and split simulated data compared to Smits simulated data at 12 hours.

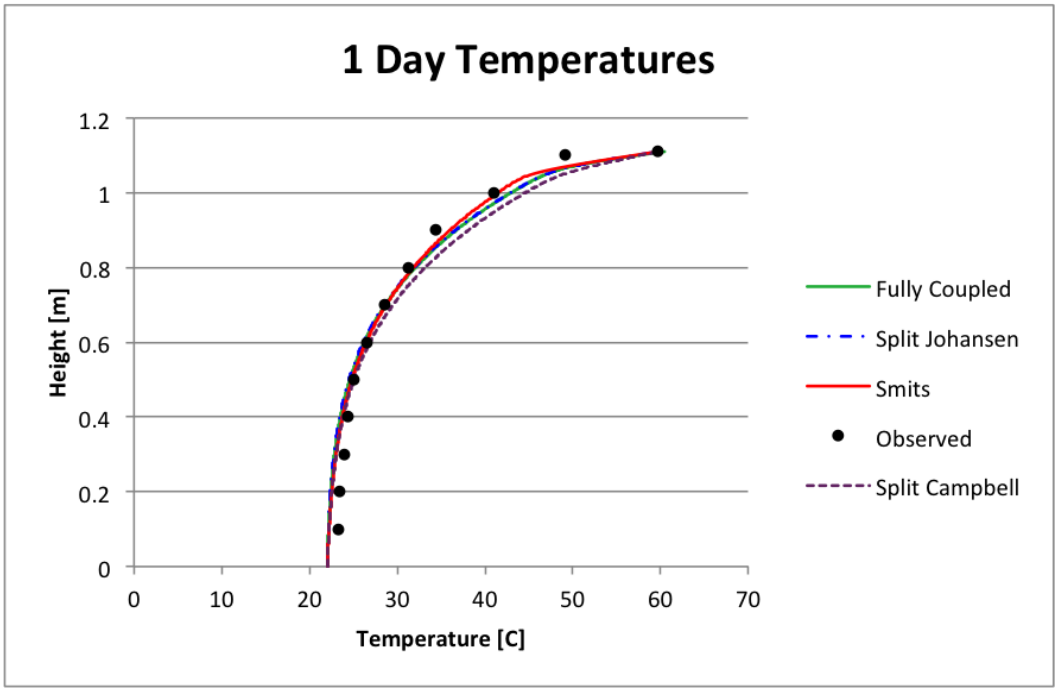

Figure 6.7

Fully coupled and split simulated data compared to Smits simulated and observed data at 1 day.

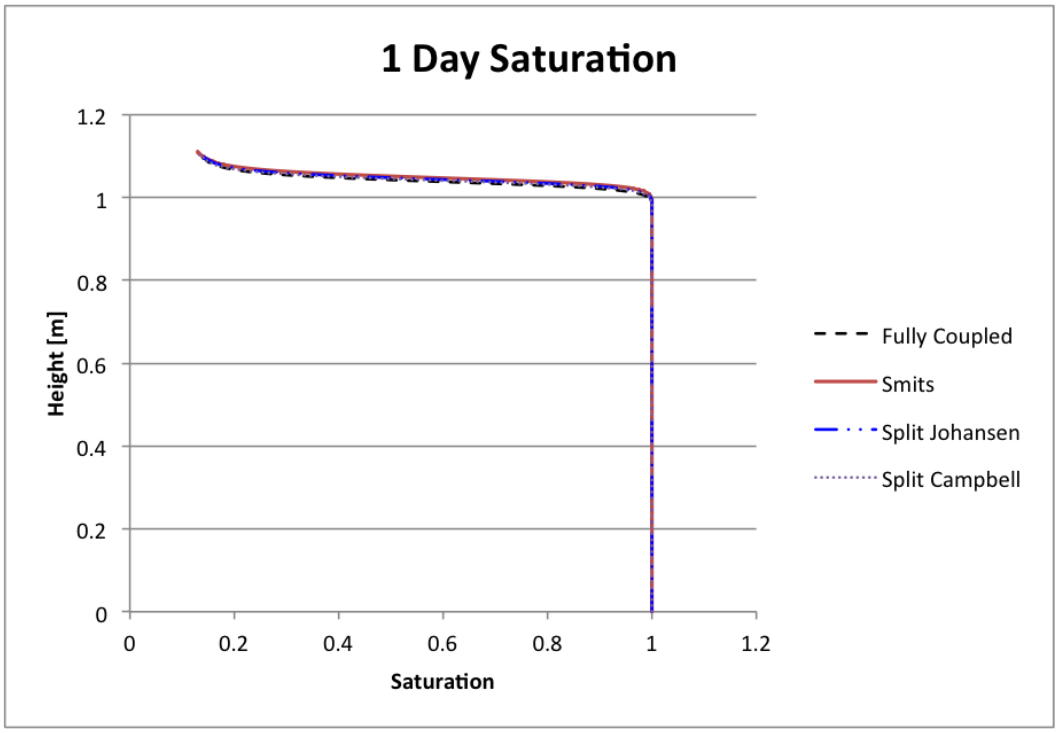

Figure 6.8

Fully coupled and split simulated data compared to Smits simulated and observed data at 1 day.

CHAPTER 7

CONCLUSIONS

A fully coupled and sequential split operator approach for modeling two-phase air-water flow and heat transport have been implemented in the Proteus Computational Methods and Simulation Toolkit. The approaches have been compared to each other as well as to data collected and simulated by Smits et. al. The sequential split operator approach has shown to be a good alternative to the fully coupled implementation for this specific problem, evaporation with little or no wetting phase flow. The solution errors were at most within 10e-1 of each other and the fully coupled approach took approximately 3.5 times longer to run than the split operator implementation.

The comparison of the Johansen and Campbell et al. thermal conductivity models in the split formulation show that the Johansen model, which is often used in vadose zone simulations, actually matches the data better than the Campbell model. However, this may not be the case over time as the evaporation continues further down in the column. Future work will include running the simulations over the full observed time of 32 days. Also, higher order time integration schemes and iterative splitting methods should be examined to see if the temporal and splitting errors can be reduced further. Restrictive boundary conditions were used for the simulations, namely the dirichlet conditions for temperature

and water vapor mass fraction. It would be interesting to test flux boundary conditions at the top of the column for the temperature and water vapor mass fraction components.

REFERENCES

[1] N. E. Bixler, *NORIA - A finite element computer program for analyzing water, vapor, air, and energy transport in porous media*, technical report SAND84-2057, Sandia National Laboratories, Albuquerque, New Mexico, August 1985.

[2] R. H. Brooks and A. T. Corey, "Hydraulic properties of porous media," *Hydrology Paper*, vol. 26, 2003, pp. 373–394.

[3] G. S. Campbell, *Soil Physics with BASIC: Transport Models for Soil-Plant Systems*, Elsevier, Amsterdam, 1985.

[4] A. Cass, G. S. Campbell, and T. L. Jones, "Enhancement of thermal water-vapor diffusion in soil," *Soil Science Society of America*, vol. 48, 1984, pp. 25–32.

[5] M. A. Celia, E. T. Bouloutas, and R. L. Zarba, "A general mass-conservative numerical solution for the unsaturated flow equation," *Water Resources Research*, vol. 26, no. 7, July 1990, pp. 1483–1496.

[6] M. W. Farthing, C. E. Kees, and C. T. Miller, "Mixed finite element methods and higher order temporal approximations for variable saturated groundwater flow," *Advances in Water Resources*, vol. 26, 2003, pp. 373–394.

[7] R. A. Freeze and J. A. Cherry, *Groundwater*, Prentice Hall, Upper Saddle River, NH 07458, 1979.

[8] S. E. Gasda, M. W. Farthing, C. E. Kees, and C. T. Miller, "Adaptive split-operator methods for modeling transport phenomena in porous medium systems," *Advances in Water Resources*, vol. 34, 2011, pp. 1268–1282.

[9] M. T. V. Genuchten, "A closed-form equation for predicting the hydraulic conductivity of unsaturated soils," *Soil Science Society of America Journal*, vol. 44, no. 5, 1980, pp. 892–8.

[10] J. Grifoll, J. M. Gasto, and Y. Cohen, "Non-isothermal soil water transport and evaporation," *Advances in Water Resources*, vol. 28, no. 11, 2005, pp. 1254–1266.

[11] R. Helmig, *Multiphase Flow and Transport Processes in the Subsurface*, Springer, New York, 1997.

[12] D. Hillel, *Fundamentals of Soil Physics*, Academic Press, San Diego, California, 1980.

[13] C. E. Kees and C. T. Miller, "Higher order time integration methods for two-phase flow," *Advances in Water Resources*, vol. 25, 2002, pp. 159–177.

[14] D. R. Lide, *CRC Handbook of Chemistry and Physics*, 73rd edition, CRC Press, Boca Raton, Florida, 1992.

[15] J. L. Monteith and M. Unsworth, *Principles of Environmental Physics*, 2 edition, Routledge Chapman and Hall, New York, 1990.

[16] Y. Mualem, "A new model for predicting the hydraulic conductivity of unsaturated porous media," *Water Resources Research*, vol. 12, no. 3, 1976, pp. 513–22.

[17] C. D. Peters-Lidard, E. Blackburn, X. Liang, and E. F. Wood, "The Effect of Soil Thermal Conductivity Parameterization on Surface Energy Fluxes and Temperatures," *Journal of the Atmospheric Sciences*, vol. 55, 1998, pp. 1209–1224.

[18] "Proteus Computational Methods and Simulation Toolkit," Internet: http://proteus.usace.army.mil/, 2012.

[19] L. A. Richards, "Capillary conduction of liquids through porous media," *Physics*, vol. 1, 1931, pp. 318–333.

[20] H. Saito, J. imnek, and B. P. Mohanty, "Numerical Analysis of Coupled Water, Vapor, and Heat Transport in the Vadose Zone," *Vadose Zone Journal*, vol. 5, no. 2, 2006, pp. 784–800.

[21] H. She and B. E. Sleep, "Effect of temperature on capillary pressure-saturation relationships for air-water and perchloroethylene-water systems," *Water Resources Research*, vol. 34, 1998, pp. 2587–2597.

[22] K. M. Smits, A. Cihan, T. Sakaki, and T. H. Illangasekare, "Evaporation from soils under thermal boundary conditions: Experimental and modeling investigation to compare equilibrium- and nonequilibrium-based approaches," *Water Resources Research*, vol. 47, no. 5, 2011, pp. 1–14.